



Formation of CO through C ($2s^22p^2\ ^3P$) and O ($2s^22p^4\ ^3P$) Radiative Association

Han Meng^{1,2}, Zhi Qin^{1,2}, and Linhua Liu^{1,2,3}¹ School of Energy and Power Engineering, Shandong University, Jinan, 250061, People's Republic of China; z.qin@sdu.edu.cn, liulinhua@sdu.edu.cn² Optics and Thermal Radiation Research Center, Institute of Frontier and Interdisciplinary Science, Shandong University, Qingdao 266237, People's Republic of China³ School of Energy Science and Engineering, Harbin Institute of Technology, Harbin 150001, People's Republic of China

Received 2022 April 13; revised 2022 July 13; accepted 2022 July 14; published 2022 August 23

Abstract

The formation of CO through the radiative association of the carbon (C, $2s^22p^2\ ^3P$) and oxygen (O, $2s^22p^4\ ^3P$) atoms is investigated. The corresponding cross sections and rate coefficients for temperatures $T=10\text{--}10,000$ K are calculated using the quantum-mechanical approach based on ab initio potential energy curves, permanent dipole moments, and transition dipole moments, which are obtained by the internally contracted multi-reference configuration interaction method with the Davidson correction and aug-cc-pwCV5Z-DK basis set. All dipole-allowed transitions between singlet, triplet, and quintet states converging to the C ($2s^22p^2\ ^3P$) + O ($2s^22p^4\ ^3P$) dissociation limit are considered. Compared to the previous results that only contain the $X^1\Sigma^+ \rightarrow X^1\Sigma^+$, $A^1\Pi \rightarrow X^1\Sigma^+$, and $B^1\Sigma^+ \rightarrow X^1\Sigma^+$ transitions, our results suggest that the $a^3\Sigma^+ \rightarrow a^3\Pi$ and $d^3\Delta \rightarrow a^3\Pi$ transitions make significant contributions to the radiative association for $T=10\text{--}30$ K. The total rate coefficient at low temperatures is estimated to be about $10^{-18}\text{ cm}^3\text{ s}^{-1}$, which shows significant deviation from the previous results, where only three transitions were considered. New rate coefficients may improve the chemical modeling of CO in the low-density region of the interstellar medium.

Unified Astronomy Thesaurus concepts: [Astrochemistry \(75\)](#); [Interstellar molecules \(849\)](#); [Radiative processes \(2055\)](#)

Supporting material: machine-readable tables

1. Introduction

Carbon monoxide (CO) is one of the most plentiful polar molecules in the interstellar medium. Thus, the rate coefficient for CO formation through various mechanisms is critical in astrochemistry. As a mechanism for molecule formation, radiative association plays an important role in the chemical evolution of small molecules detected in supernovae (Liu & Dalgarno 1994), novae (Rawlings 1988), molecular outflow regions (Glassgold et al. 1991), interstellar clouds (Herbst & Bates 1988), and stellar atmospheres (Langer & Glassgold 1990; Glassgold 1996). In particular, the formation of CO through the radiative association of C ($2s^22p^2\ ^3P$) and O ($2s^22p^4\ ^3P$) is the primary source of CO in the supernova 1987A (Dalgarno et al. 1990).

Radiative association is a process where a molecule forms by the association of two colliding fragments with spontaneous emission of a photon. Experimentally, radiative association is difficult to measure and only in a few cases have rate coefficients been successfully measured. This was primarily implemented using ion traps or the ion cyclotron resonance apparatus, requiring that at least one of the colliding species is charged. Therefore, no experimental results for the formation of neutral diatomic molecules through radiative association are available (Nyman et al. 2015). However, there are many traditional theories and methods to compute cross sections and rate coefficients of the radiative association, such as the semi-empirical method, classical approach, Breit–Wigner theory, optical potential approach, and quantum-mechanical approach.

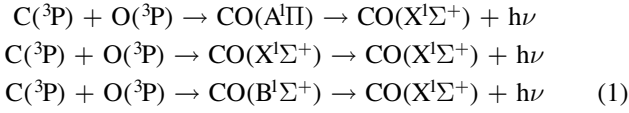
These theories and methods of radiative association for diatomic molecules and ions are well established and summarized in the work of Nyman et al. (2015), and have been used for dealing with many diatomic molecules and ions, such as CO (Gustafsson & Nyman 2015), PO (Andreazza et al. 2016), SiO (Cairnie et al. 2017), CS (Forrey et al. 2018), CO^+ (Zámečníková et al. 2020), MgO (Bai et al. 2021), N_2^+ (Qin et al. 2021), AlO (Bai et al. 2022), etc. In addition, recent developments in the theories and methods for radiative association include the Sturmian quantum kinetic theory (Forrey 2015), the surface-hopping model of spontaneous electronic transitions (Szabó & Gustafsson 2017), the extension of radiative association for local thermal equilibrium (Gustafsson & Forrey 2019), and the treatment of non-adiabatic couplings (Gustafsson 2020).

Each of the two atoms, C and O, has nine microstates in their electronic ground states labeled by the spin and orbital angular momentum quantum numbers, resulting in a total of $9 \times 9 = 81$ molecule states. In the radiative association of C ($2s^22p^2\ ^3P$) and O ($2s^22p^4\ ^3P$), the atoms can approach each other in any of the 81 molecular states, including two Σ^+ states, one Σ^- state, two Π states, and one Δ state, each of them with total electronic spin multiplicities of singlet, triplet, and quintet. An early estimate for the temperature-independent rate coefficient of the CO radiative association was given by Julienne & Krauss (1973) as $10^{-17}\text{ cm}^3\text{ s}^{-1}$. Later, Dalgarno et al. (1990) discussed the contribution of various states to the CO radiative association and concluded that the main contribution comes from the ground state $X^1\Sigma^+$ and the first excited state $A^1\Pi$. Subsequently, Gustafsson & Nyman's (2015) research group applied the quantum-mechanical approach to compute the rate coefficients of the CO radiative association by considering one more excited $B^1\Sigma^+$ state, i.e., the

Table 1
Transitions Studied in this Work

Continuum	To	Bound	Continuum	To	Bound	Continuum	To	Bound
$X^1\Sigma^+$	\rightarrow	$X^1\Sigma^+$	$A^1\Pi$	\rightarrow	$D^1\Delta$	$c^3\Pi$	\rightarrow	$a^3\Sigma^+$
$A^1\Pi$	\rightarrow	$X^1\Sigma^+$	$D^1\Delta$	\rightarrow	$D^1\Delta$	$a^3\Pi$	\rightarrow	$d^3\Delta$
$B^1\Sigma^+$	\rightarrow	$X^1\Sigma^+$	$E^1\Pi$	\rightarrow	$D^1\Delta$	$d^3\Delta$	\rightarrow	$d^3\Delta$
$E^1\Pi$	\rightarrow	$X^1\Sigma^+$	$E^1\Pi$	\rightarrow	$B^1\Sigma^+$	$c^3\Pi$	\rightarrow	$d^3\Delta$
$X^1\Sigma^+$	\rightarrow	$A^1\Pi$	$a^3\Pi$	\rightarrow	$a^3\Pi$	$a^3\Pi$	\rightarrow	$e^3\Sigma^-$
$A^1\Pi$	\rightarrow	$A^1\Pi$	$a^3\Sigma^+$	\rightarrow	$a^3\Pi$	$e^3\Sigma^-$	\rightarrow	$e^3\Sigma^-$
$I^1\Sigma^-$	\rightarrow	$A^1\Pi$	$d^3\Delta$	\rightarrow	$a^3\Pi$	$c^3\Pi$	\rightarrow	$e^3\Sigma^-$
$D^1\Delta$	\rightarrow	$A^1\Pi$	$e^3\Sigma^-$	\rightarrow	$a^3\Pi$	$1^5\Pi$	\rightarrow	$1^5\Pi$
$B^1\Sigma^+$	\rightarrow	$A^1\Pi$	$b^3\Sigma^+$	\rightarrow	$a^3\Pi$	$1^5\Sigma^+$	\rightarrow	$1^5\Pi$
$E^1\Pi$	\rightarrow	$A^1\Pi$	$c^3\Pi$	\rightarrow	$a^3\Pi$	$1^5\Sigma^-$	\rightarrow	$1^5\Pi$
$A^1\Pi$	\rightarrow	$I^1\Sigma^-$	$a^3\Pi$	\rightarrow	$a^3\Sigma^+$	$1^5\Delta$	\rightarrow	$1^5\Pi$
$I^1\Sigma^-$	\rightarrow	$I^1\Sigma^-$	$a^3\Sigma^+$	\rightarrow	$a^3\Sigma^+$	$2^5\Sigma^+$	\rightarrow	$1^5\Pi$
$E^1\Pi$	\rightarrow	$I^1\Sigma^-$	$b^3\Sigma^+$	\rightarrow	$a^3\Sigma^+$	$2^5\Pi$	\rightarrow	$1^5\Pi$

radiative association reactions



had been computed (Franz et al. 2011; Antipov et al. 2013; Gustafsson & Nyman 2015).

In this work, we have considered all the radiative association processes of the C ($2s^2 2p^2 \ ^3P$) and O ($2s^2 2p^4 \ ^3P$) colliding atoms, as depicted in Table 1. A total of 18 electronic states are generated and their potential energy curves (PECs), permanent dipole moments (PDMs), and dipole-allowed transition dipole moments (TDMs) are calculated by a state-of-the-art ab initio method. Then, the PECs, PDMs, and TDMs are used to compute the cross sections by the quantum-mechanical approach, which treats the nuclear wave functions quantum mechanically and consequently takes complete account of tunneling effects and resonances. Finally, the rate coefficients are computed based on the cross sections and fitted to an analytical formula.

2. Theory and Methods

2.1. PECs and TDMs

Using the high-level ab initio calculations implemented in the MOLPRO 2015 software package (Werner et al. 2015, 2020), the electronic structures of CO have been determined. In our calculations, the molecular orbitals (MOs) and ground-state energies are computed by the HF method. Then, the CASSCF method (Knowles & Werner 1985; Werner & Knowles 1985) is applied to perform the state-averaged calculation to generate multi-configuration wave functions by utilizing the HF MOs as the starting orbitals. Finally, based on the CASSCF wave functions, the internally contracted multi-reference configuration interaction method with the Davidson correction (icMRCI+Q) (Knowles & Werner 1988; Werner et al. 1988; Knowles & Werner 1992; Shamasundar et al. 2011) is performed to consider the dynamic correlation and size-consistency error. The augmented correlation consistent polarized weighted core valence quintuplet aug-cc-pwCV5Z-DK Gaussian basis set is selected to describe the carbon and oxygen atoms, which is found to give an excellent production of the potential energy and dipole moments for electronic states as the CO molecule dissociates, as mentioned in previous publications (Dunning 1989; De Jong et al. 2001; Peterson & Dunning 2002). The

Table 2
The Grid of Energies for the Quantum Scattering Calculation

Energy Interval (cm^{-1})	Step Size (cm^{-1})
0.008–0.01	0.0001
0.01–0.02	0.0002
0.02–0.08	0.0005
0.08–0.17	0.001
0.17–1	0.005
1–2	0.025
2–20	0.05
20–60	0.25
60–100	0.5
100–200	1
200–1000	5
1000–10,000	10
10,000–15,000	20
15,000–85,000	50

scalar relativistic effect is considered by the third-order Douglas–Kroll Hamiltonian approximation (Reiher & Wolf 2004, 2004). The PECs, PDMs, and TDMs for the singlet and triplet states were computed at the internuclear distances from 0.8–7.5 Å with step sizes of 0.05 Å for 0.8–0.9 Å, 0.02 Å for 0.9–1.5 Å, 0.05 Å for 1.5–2.6 Å, 0.1 Å for 2.6–6 Å, and 0.5 Å for 6–7.5 Å, and those for the quintet states were computed at the internuclear distances from 0.8–15 Å with step sizes of 0.05 Å for 0.8–0.9 Å, 0.02 Å for 0.9–1.5 Å, 0.05 Å for 1.5–2.6 Å, 0.1 Å for 2.6–6 Å, and 0.5 Å for 6–15 Å. The obtained PECs can be also used to determine the dissociation energy D_e , the electronic excitation energy relative to the ground state T_e , the internuclear separation R_e , the harmonic frequency ω_e , the first-order anharmonic constant $\omega_e\chi_e$, the rotational constant B_e , and the vibrational coupling constant α_e .

MOLPRO cannot take advantage of the full symmetry of non-Abelian groups, so an Abelian subgroup is often adopted for computing molecular properties. In this work, four inner electrons of CO are placed into two closed-shell MOs in the irreducible representations of C_{2v} : two a_1 orbitals, no b_1 orbital, no b_2 orbital, and no a_2 orbital. The remaining 10 electrons are placed into 12 outermost MOs, which constitute the active space: six a_1 orbitals, three b_1 orbitals, three b_2 orbitals, and no a_2 orbital. The orbitals of active space are called (6, 3, 3, 0).

To calculate the cross sections and rate coefficients of the CO radiative association, PECs, PDMs, and TDMs must be extrapolated over the short-range and long-range internuclear

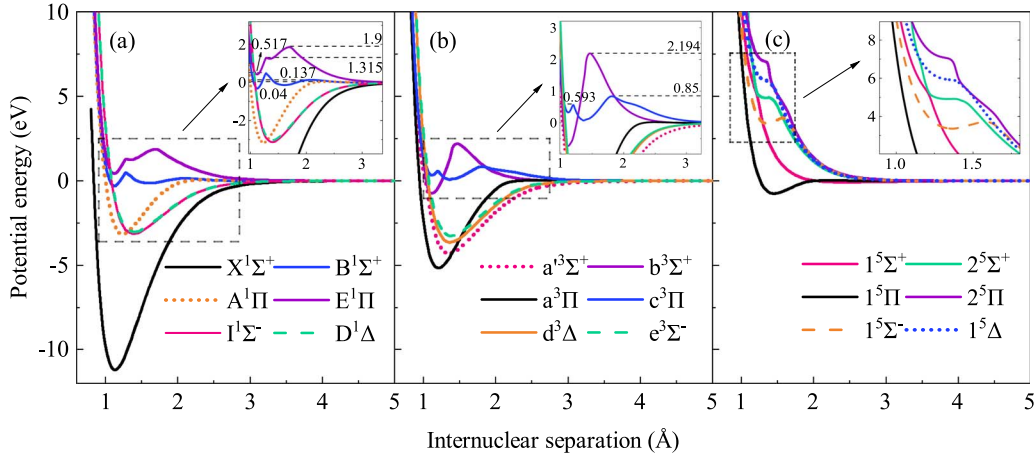


Figure 1. Potential energy curves of the (a) singlet, (b) triplet, and (c) quintet states for CO calculated at the icMRCI+Q/aug-cc-pwCV5Z-DK level of theory.

separations R . In this work, PECs in the short-range regions ($R < 0.8 \text{ \AA}$) are extrapolated by the following function:

$$V(R) = A \exp(-BR) + C, \quad (2)$$

where A , B , and C are fitting parameters. For long-range internuclear separations (i.e., $R > 7.5 \text{ \AA}$ for the singlet and triplet states and $R > 15 \text{ \AA}$ for the quintet states), the PECs can be extrapolated by the following function:

$$V(R) = -\frac{C_5}{R^5} - \frac{C_6}{R^6} + V(R \rightarrow \infty), \quad (3)$$

where C_5 and C_6 are coefficients for each electronic state. In this work, C_5 and C_6 were estimated by fitting ab initio points while keeping the dissociation limits fixed. The same extrapolation is used for PDMs and TDMs. Noted that extrapolating the TDMs of the $a^3\Sigma^+ - a^3\Pi$ involves uncertainty due to the large slope, but it has a negligible effect on the calculation of the cross sections and rate coefficients.

2.2. Radiative Associative Cross Sections and Rate Coefficients

The quantum-mechanical cross section for the radiative association process can be expressed as the sum of the state-resolved cross sections $\sigma_{\Lambda', J' \rightarrow \Lambda'', v'', J''}(E)$ for the transitions $\Lambda', J' \rightarrow \Lambda'', v'', J''$ (Babb & Dalgarno 1995).

$$\begin{aligned} \sigma_{\Lambda' \rightarrow \Lambda''}(E) &= \sum_{J', v'', J''} \sigma_{\Lambda', J' \rightarrow \Lambda'', v'', J''}(E) \\ &= \sum_{J', v'', J''} \frac{1}{4\pi\epsilon_0} \frac{64 \pi^5}{3 k^2} p_{\Lambda'} \\ &\quad \times \left(\frac{\nu}{c}\right)^3 S_{\Lambda', J' \rightarrow \Lambda'', v'', J''} |M_{\Lambda', E, J'; \Lambda'', v'', J''}|^2, \end{aligned} \quad (4)$$

where ν and J denote the quantum numbers of vibrations and rotations, respectively. Λ represents the absolute value of the projection of the electronic orbital angular momentum on the internuclear axis. Therefore, $\Lambda = 0, 1$, and 2 represent the Σ, Π , and Δ states, respectively. Single prime and double prime refer to upper and lower energy levels, respectively. ϵ_0 is the vacuum permittivity, $k^2 = 2\mu E/\hbar^2$, and \hbar is the reduced Planck constant. Furthermore, ν denotes the frequency of the emitted photon, c denotes the speed of light in a vacuum, and $S_{\Lambda', J' \rightarrow \Lambda'', v'', J''}$ is the Hönl–London factor of the transition

$\Lambda', J' \rightarrow \Lambda'', v'', J''$. Hönl–London factors are the factors that give the dependence of spectroscopic line intensities on the rotational quantum numbers and are obtained based on Hansson & Watson (2005) and Watson (2008), as follows:

$$\begin{aligned} S_{\Lambda', J' \rightarrow \Lambda'', v'', J''} &= \begin{cases} \Delta\Lambda = 0, & \frac{(J'' + \Lambda'')(J'' - \Lambda'')}{J''}, \\ \Delta\Lambda = +1, & \frac{(J'' - 1 - \Lambda'')(J'' - \Lambda'')}{4J''}, \text{ (P-branch)} \\ \Delta\Lambda = -1, & \frac{(J'' - 1 + \Lambda'')(J'' + \Lambda'')}{4J''}, \end{cases} \\ S_{\Lambda', J' \rightarrow \Lambda'', v'', J''} &= \begin{cases} \Delta\Lambda = 0, & \frac{(2J'' + 1)\Lambda''^2}{J''(J'' + 1)}, \\ \Delta\Lambda = +1, & \frac{(J'' + 1 + \Lambda'')(J'' - \Lambda'')(2J'' + 1)}{4J''(J'' + 1)}, \text{ (Q-branch)} \\ \Delta\Lambda = -1, & \frac{(J'' + 1 - \Lambda'')(J'' + \Lambda'')(2J'' + 1)}{4J''(J'' + 1)}, \end{cases} \\ S_{\Lambda', J' \rightarrow \Lambda'', v'', J''} &= \begin{cases} \Delta\Lambda = 0, & \frac{(J'' + 1 + \Lambda'')(J'' + 1 - \Lambda'')}{J'' + 1}, \\ \Delta\Lambda = +1, & \frac{(J'' + 2 + \Lambda'')(J'' + 1 + \Lambda'')}{4(J'' + 1)}, \text{ (R-branch)} \\ \Delta\Lambda = -1, & \frac{(J'' + 2 - \Lambda'')(J'' + 1 - \Lambda'')}{4(J'' + 1)}, \end{cases} \end{aligned} \quad (5)$$

$p_{\Lambda'}$ is the statistical weight or the probability of collision in the initial electronic state Λ' , given by

$$p_{\Lambda'} = \frac{(2S + 1)(2 - \delta_{0, \Lambda'})}{(2L_C + 1)(2S_C + 1)(2L_O + 1)(2S_O + 1)}, \quad (6)$$

where δ is the Kronecker delta function, S is the spin quantum number of the initial electronic state, L_C and S_C are the electronic orbital angular momentum and spin quantum number of the carbon atom, respectively, similarly, L_O and S_O are the electronic orbital angular momentum and spin quantum number

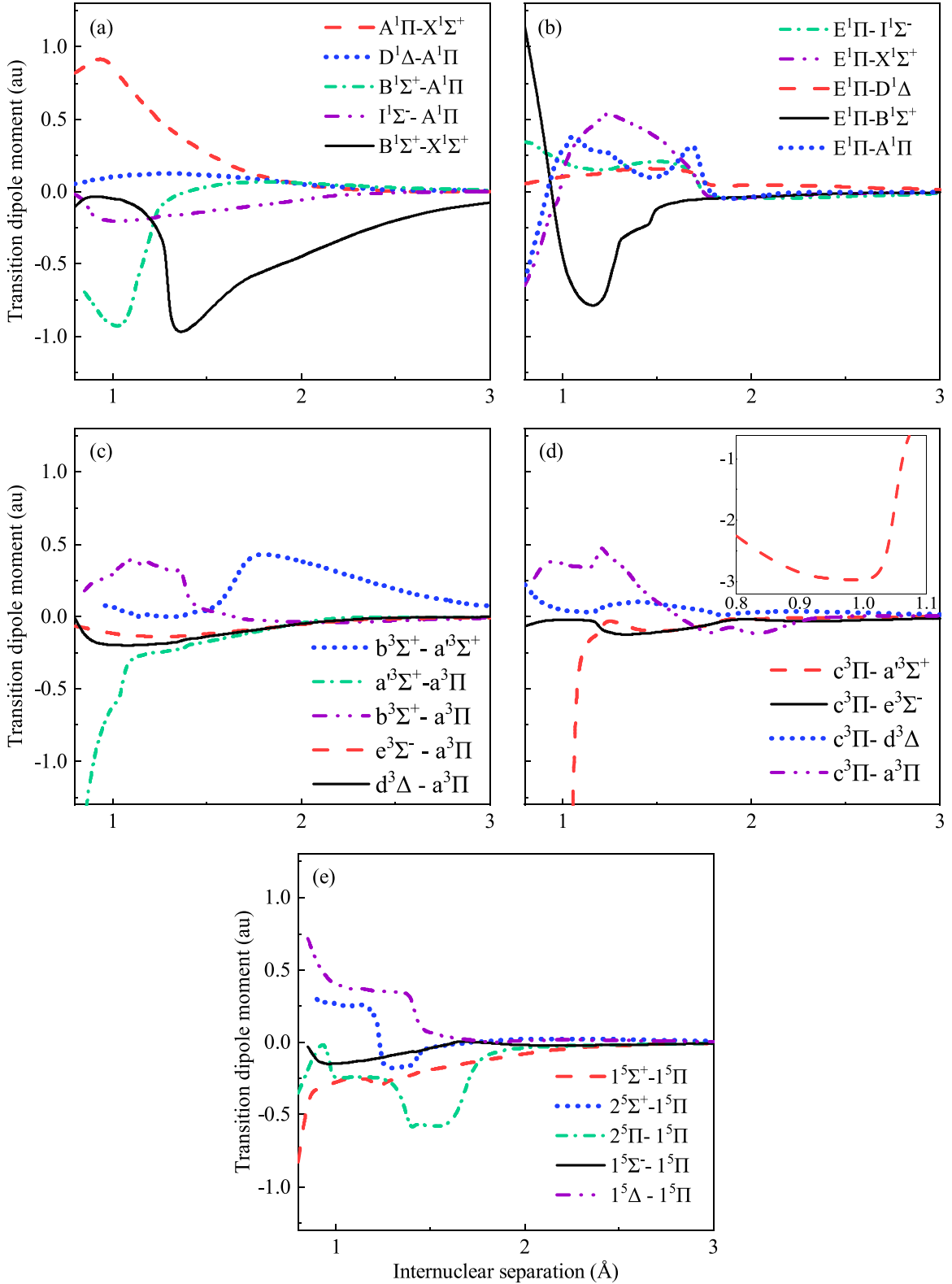


Figure 2. Transition dipole moments for the (a), (b) singlet, (c), (d) triplet, and (e) quintet transitions of CO.

of the oxygen atom, respectively. $M_{\Lambda', E, J'; \Lambda'', v'', J''}$ is the radial matrix element, given by

$$M_{\Lambda', E, J'; \Lambda'', v'', J''} = \int_0^\infty \chi_{E, J'}^{\Lambda'}(R) D_{\Lambda' \Lambda''}(R) \psi_{v'', J''}^{\Lambda''}(R) dR, \quad (7)$$

where $\chi_{E, J'}^{\Lambda'}(R)$ is the radial wave function of the initial continuum state, $\psi_{v'', J''}^{\Lambda''}(R)$ is the radial wave function of the rovibrational bound state, and $D_{\Lambda' \Lambda''}(R)$ is the PDM for the transition dipole radiation or TDM for the permanent dipole radiation. We considered all the bound rovibrational levels

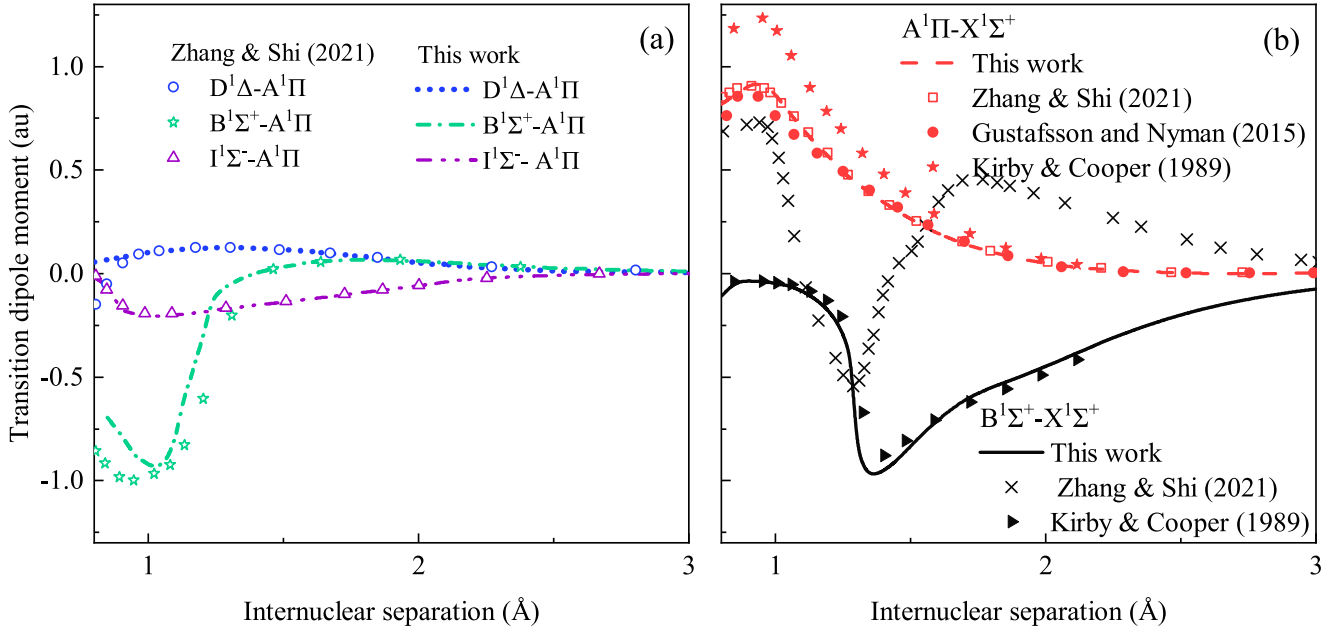


Figure 3. TDMs for the singlet, triplet, and quintet states of CO. (a) Comparison of the $D^1\Delta \rightarrow A^1\Pi$, $B^1\Sigma^+ \rightarrow A^1\Pi$, and $I^1\Sigma^- \rightarrow A^1\Pi$ with those computed by Zhang & Shi (2021). (b) Comparison of the $A^1\Pi \rightarrow X^1\Sigma^+$ and $B^1\Sigma^+ \rightarrow X^1\Sigma^+$ with those computed by Kirby & Cooper (1989), Franz et al. (2011), and Zhang & Shi (2021).

below the dissociation limit, so we chose an appropriate energy resolution that can reproduce the resonances as much as possible and save computation cost. The grid of energies is given in Table 2. The bound and continuum wave functions are obtained by the renormalized Numerov method (Johnson 1977, 1978) with a step size of 0.001 cm^{-1} .

The rate coefficients can be obtained from the radiative association cross sections. In the spin-free approximation, the rate coefficients can be expressed as a function of temperature T ,

$$\alpha_{\Lambda' \rightarrow \Lambda''}(T) = \left(\frac{8}{\mu\pi}\right)^{\frac{1}{2}} \left(\frac{1}{k_B T}\right)^{\frac{3}{2}} \int_0^\infty E \sigma_{\Lambda', J' \rightarrow \Lambda'', v'', J''}(E) e^{-\frac{E}{k_B T}} dE, \quad (8)$$

where μ is the reduced mass of CO, k_B is the Boltzmann constant, and E is the collision energy. The total thermal rate coefficient for the formation of CO can be expressed as

$$\alpha_{\text{tot}}(T) = \sum_{\Lambda' \rightarrow \Lambda''} \alpha_{\Lambda' \rightarrow \Lambda''}(T). \quad (9)$$

3. Results and Discussion

3.1. PECs and TDMs

The PECs of 18 electronic states for CO are calculated at the icMRCI+Q/aug-cc-pwCV5Z-DK level of theory and displayed in Figure 1 as a function of the internuclear separation R . The 18 electronic states of CO are dissociated to the C ($2s^2 2p^2 \ ^3P$) and O ($2s^2 2p^4 \ ^3P$) dissociation limit. The $B^1\Sigma^+$ state has two shallow potential wells. Both $E^1\Pi$ and $c^3\Pi$ states also have two potential wells that are above the dissociation limit. The $b^3\Sigma^+$, $1^5\Sigma^-$, and $2^5\Sigma^+$ states have one potential well in which the latter two are above the dissociation limit. The $1^5\Delta$ and $2^5\Pi$ states are repulsive but decrease very slowly at the internuclear separations $R = 1.24\text{--}1.36 \text{ \AA}$. Other electronic states are bound. The PECs of $I^1\Sigma^-$ and $D^1\Delta$ are incredibly

similar because the electronic configurations of both states have almost the same weight at each R . To verify the accuracy of the PECs, the fitted spectroscopic constants are compared with previous experimental and theoretical ones. For the $X^1\Sigma^+$, $a^3\Pi$, $a^3\Sigma^+$, $d^3\Delta$, $e^3\Sigma^-$, $A^1\Pi$, $I^1\Sigma^-$, $D^1\Delta$, and $B^1\Sigma^+$ states, our fitted spectroscopic constants agree well with those determined experimentally and theoretically. The $I^1\Sigma^-$, $D^1\Delta$, and $e^3\Sigma^-$ states have almost the same PECs, thus obtaining similar spectroscopic constants. For the $b^3\Sigma^+$, $c^3\Pi$, and $E^1\Pi$ states, except for the first-order anharmonic constant $\omega_e \chi_e$ of $E^1\Pi$, which deviates significantly from the experimentally derived value of 42.00 cm^{-1} , the rest of the spectroscopic constants are in good agreement. Quintet states have not been experimentally determined so far.

The TDMs for 24 dipole-allowed transitions of CO are calculated at the icMRCI+Q/aug-cc-pwCV5Z-DK level of theory and displayed in Figure 2. To check our TDM values, we compared our results with available ones in previous papers in Figure 3. The TDMs of four singlet systems show good agreement with those calculated by Zhang & Shi (2021) except for the $B^1\Sigma^+ \rightarrow X^1\Sigma^+$ transition. The TDM of $B^1\Sigma^+ \rightarrow X^1\Sigma^+$ agrees well with that presented by Kirby & Cooper (1989). The PDMs of the singlet, triplet, and quintet states are also computed and shown in Figure 4. Positive values correspond to polarity C^+O^+ . The PDMs for the $I^1\Sigma^-$ and $D^1\Delta$ states are very similar to each other as they have the same primary configurations at each R . The trends of PDMs for $X^1\Sigma^+$ and $A^1\Pi$ are similar to those given by Cooper & Kirby (1987). Also, the trends of PDMs for $D^1\Delta$ and $I^1\Sigma^-$ are similar to those given by Rosenkrantz & Kirby (1989), as depicted in Figure 4(a). The deviations may result from different levels of theory and basis sets.

3.2. Radiative Association Cross Sections

Among the 18 electronic states considered above, there are numerous dipole-allowed transitions. Some of the transitions, such as $B^1\Sigma^+ \rightarrow B^1\Sigma^+$, $b^3\Sigma^+ \rightarrow b^3\Sigma^+$, $1^5\Sigma^- \rightarrow 1^5\Sigma^-$, etc.,

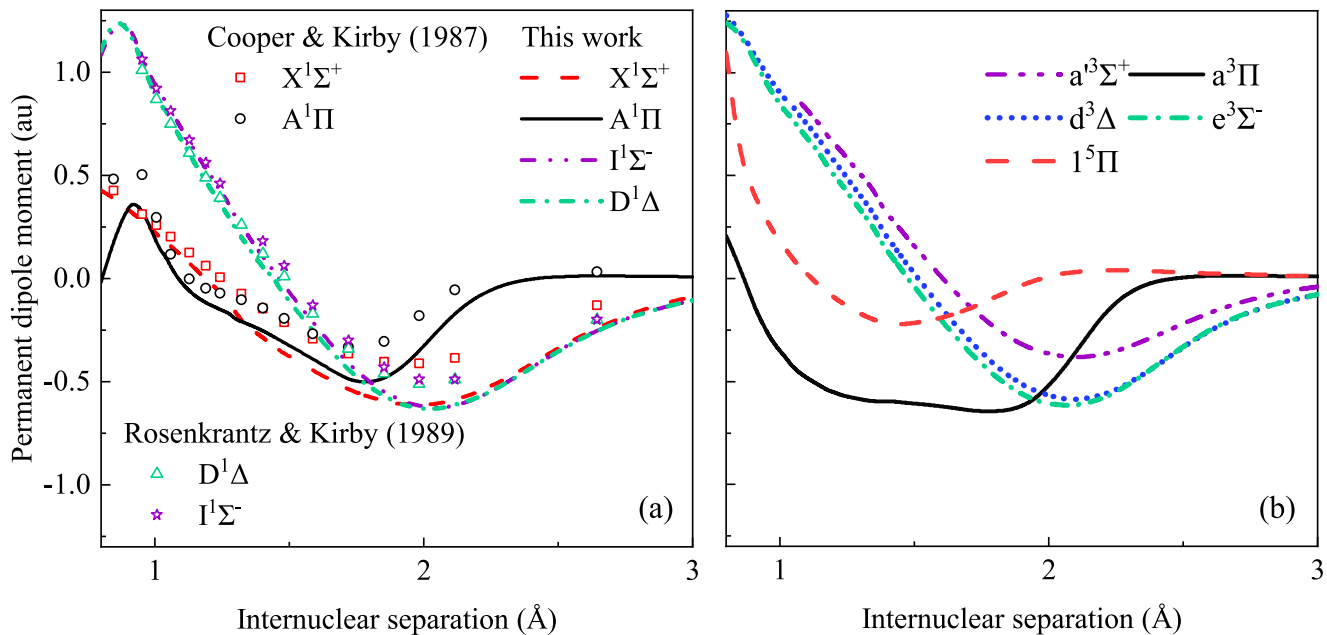


Figure 4. PDMs for the singlet, triplet, and quintet states of CO. (a) Comparison of the $X^1\Sigma^+$ and $A^1\Pi$ with those computed by Cooper & Kirby (1987), and comparison of the $D^1\Delta$ and $I^1\Sigma^-$ with those computed by Rosenkrantz & Kirby (1989). (b) Our results alone.

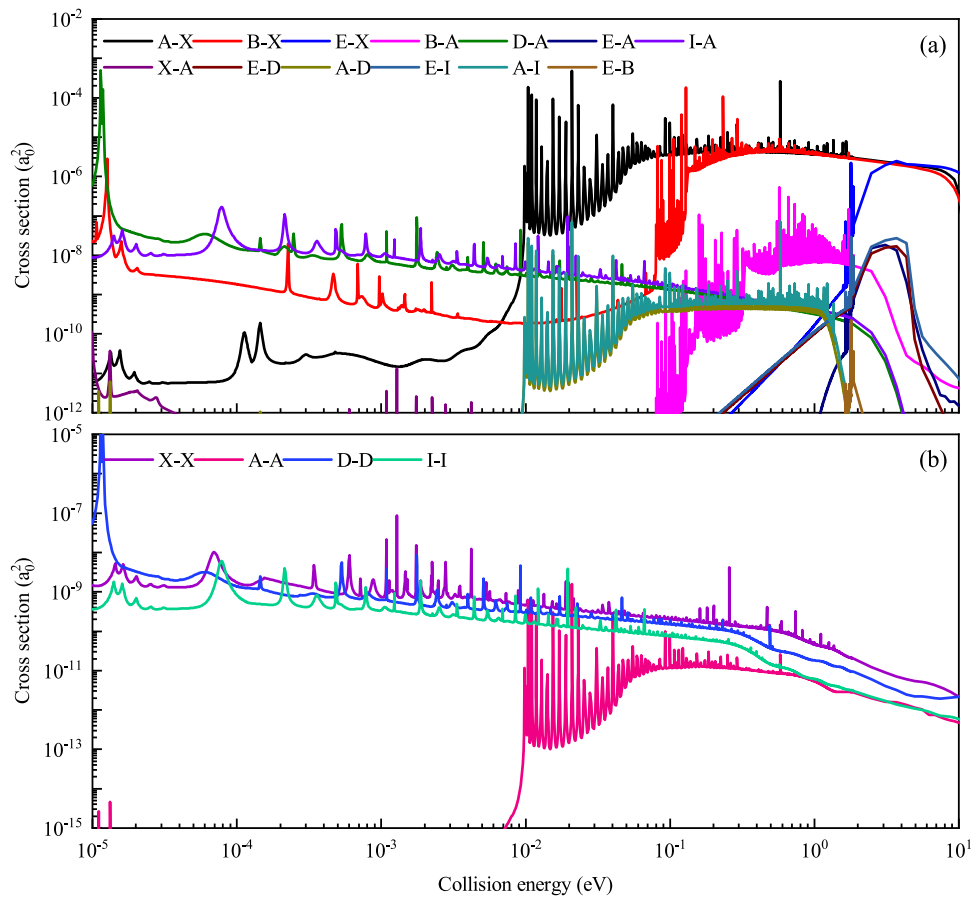


Figure 5. Radiative association cross sections as a function of the collision energy for singlet transitions. Panel (a) denotes the transition dipole radiation and panel (b) represents the permanent dipole radiation.

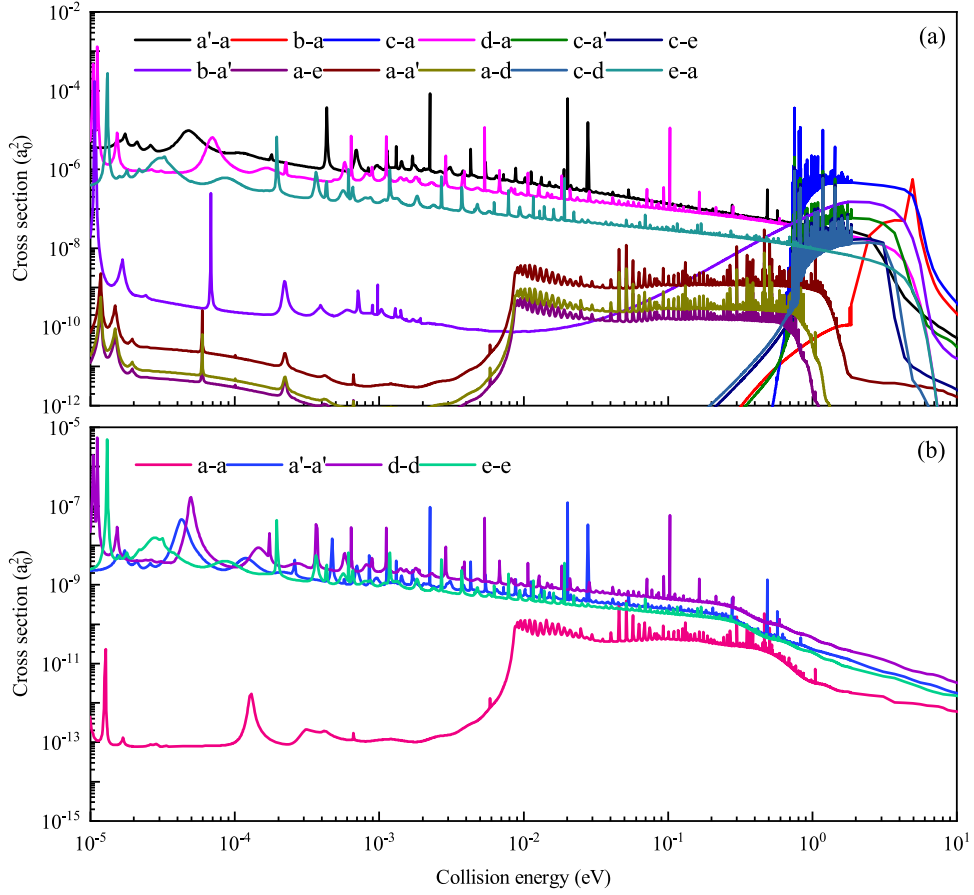


Figure 6. Radiative association cross sections as a function of the collision energy for triplet transitions. Panel (a) denotes the transition dipole radiation and panel (b) represents the permanent dipole radiation.

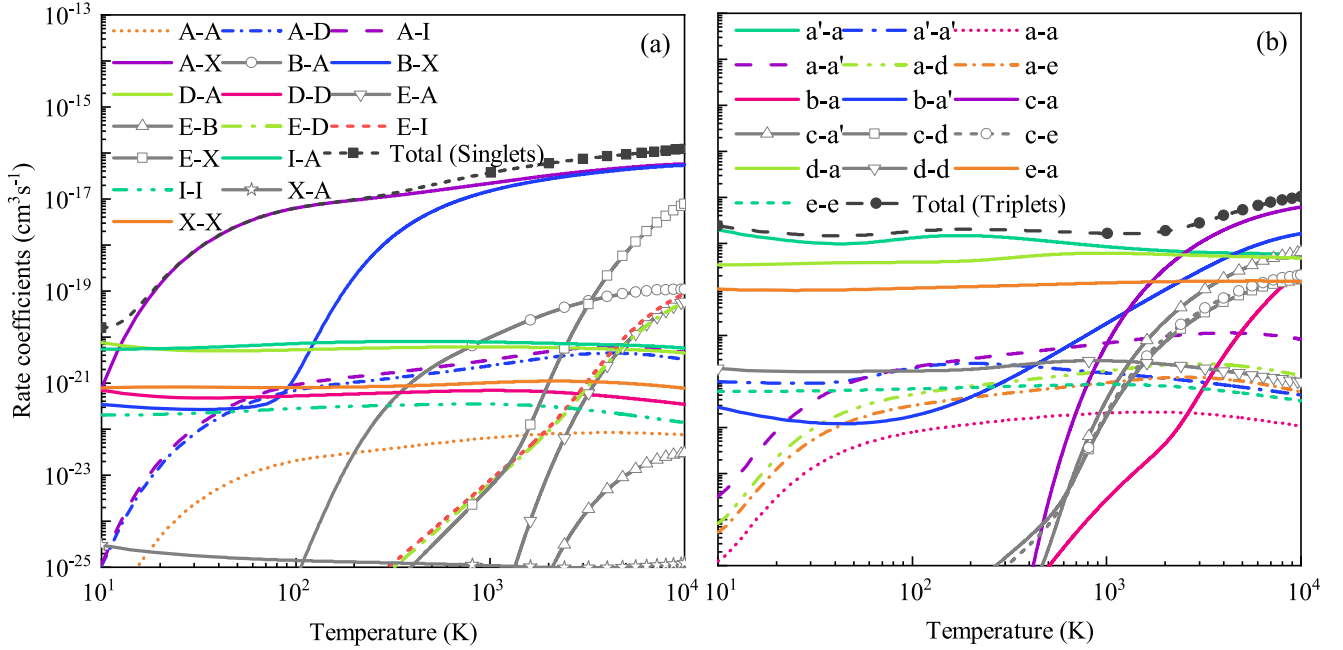


Figure 7. Rate coefficients for the radiative association of CO through the transitions between (a) singlet and (b) triplet states.

are expected to contribute little to the radiative association of C ($2s^22p^3P$) and O ($2s^22p^4^3P$) due to their shallow potential wells and are not presented here. The remaining 33 transitions are taken into account to compute their cross sections. The

results are displayed in Figures 5 and 6, and show that the cross sections exhibit numerous peaks caused by the resonances. Note that we also computed the cross sections of the $1^5\Delta \rightarrow 1^5\Pi$, $1^5\Pi \rightarrow 1^5\Pi$, $1^5\Sigma^- \rightarrow 1^5\Pi$, $1^5\Sigma^+ \rightarrow 1^5\Pi$, $2^5\Pi \rightarrow 1^5\Pi$, and

Table 3
Radiative Lifetimes (ns) of the First Seven Vibrational Levels of the $A^1\Pi$ state

v'	This Work	Calc. ^a	Calc. ^b	Calc. ^c	Expt. ^d	Expt. ^e	Expt. ^f	Expt. ^g	Expt. ^h	Expt. ⁱ
0	9.86	9.83	9.96	8.59	9.90	10.80	10.69	11.50	15.90	11.90
1	9.52	9.41	9.99	8.64	9.80	10.45	10.37	10.90	16.20	12.30
2	9.50	9.44	9.81	8.69	9.75	9.75	9.35	10.50	16.60	12.00
3	9.57	9.47	9.60	8.75	9.60	9.60	8.97	10.50	16.10	12.50
4	9.49	9.50	9.42	8.84	9.40	9.50	9.67	10.40	15.00	13.30
5	9.37	9.53	9.25	8.90	9.20	9.20	9.75	10.20	14.30	13.50
6	9.04	9.57	9.13	9.01	9.05	10.85	10.45
7	8.96	9.62	9.05	9.10	8.95	8.95

Notes.

- ^a Zhang & Shi (2021).
^b Cheng et al. (2018).
^c Kirby & Cooper (1989).
^d Eidelsberg et al. (1992).
^e Field (1983).
^f Imhof & Read (1971).
^g Hesser (1968).
^h Chervenak & Anderson (1971).
ⁱ Carlson (1978).

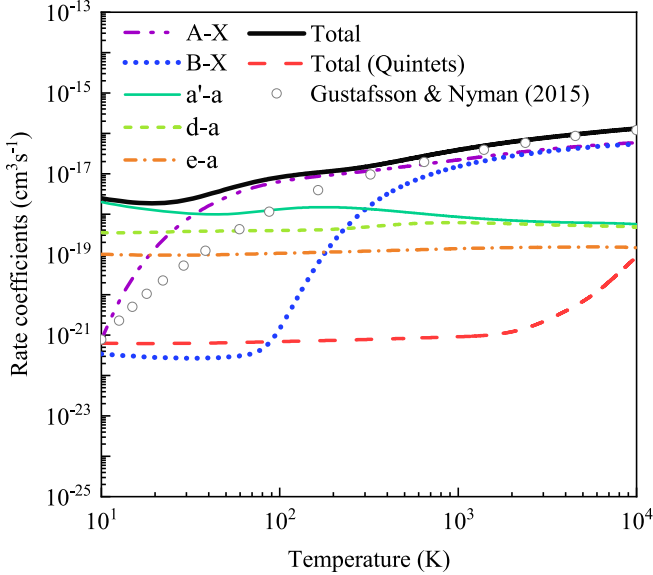


Figure 8. Rate coefficients for the radiative association of CO. “Total” denotes the total rate coefficient obtained by all transitions mentioned above, “Total (Quintets)” denotes the total rate coefficient obtained by the $1^5\Delta \rightarrow 1^5\Pi$, $1^5\Pi \rightarrow 1^5\Pi$, $1^5\Sigma^- \rightarrow 1^5\Pi$, $1^5\Sigma^+ \rightarrow 1^5\Pi$, $2^5\Pi \rightarrow 1^5\Pi$, and $2^5\Sigma^+ \rightarrow 1^5\Pi$ transitions, and “Gustafsson & Nyman (2015)” denotes the rate coefficients computed by Gustafsson & Nyman (2015) with the consideration of the $X^1\Sigma^+ \rightarrow X^1\Sigma^+$, $A^1\Pi \rightarrow X^1\Sigma^+$, and $B^1\Sigma^+ \rightarrow X^1\Sigma^+$ transitions.

$2^5\Sigma^+ \rightarrow 1^5\Pi$ transitions but found their cross sections were insignificant.

As displayed in Figures 5 and 6, the cross section for the $a^3\Sigma^+ \rightarrow a^3\Pi$ transition is dominant for the collision energies E smaller than about 0.01 eV, followed by the $d^3\Delta \rightarrow a^3\Pi$ and $e^3\Sigma^- \rightarrow a^3\Pi$ transitions. As the collision energy increases, the cross sections for some transitions, such as $A^1\Pi \rightarrow X^1\Sigma^+$, $B^1\Sigma^+ \rightarrow X^1\Sigma^+$, $c^3\Pi \rightarrow a^3\Pi$, etc., exhibit sharp jumps, which are caused by the potential barriers on the PECs of the upper states. For example, the cross section for the $c^3\Pi \rightarrow a^3\Pi$ transition rises rapidly at collision energies around 0.593 and 0.850 eV. Similar behavior can generally be found in other

Table 4
Fitting Parameters According to the Kooij Function (Equation (10)) for the Total Rate Coefficient

$T(K)$	A ($\text{cm}^3 \text{s}^{-1}$)	α	β (K)
10–20	8.3460×10^{-18}	0.9855	−22.0946
20–30	6.9342×10^{-18}	0.4947	0.3501
30–80	3.1840×10^{-17}	1.0997	4.4931
80–400	1.4973×10^{-17}	0.5706	0.2115
400–1000	1.4728×10^{-17}	0.8117	2.8737
1000–5000	2.1950×10^{-17}	0.5389	4.8882
5000–6000	2.7208×10^{-17}	0.4565	0.3054
6000–10,000	3.2299×10^{-17}	0.4005	1.5883

diatomic systems, such as the $D^1\Delta \rightarrow A^1\Pi$ transition of MgO (Bai et al. 2021), the $1^4\Sigma_g^+ \rightarrow a^4\Sigma_u^+$ transition of N_2^+ (Qin et al. 2021), and the $1^2\Delta \rightarrow A^2\Pi$ transition of AlO (Bai et al. 2022). Subsequently, the cross sections for the $A^1\Pi \rightarrow X^1\Sigma^+$ and $B^1\Sigma^+ \rightarrow X^1\Sigma^+$ transitions dominate over the energy ranges of about 0.01–10 eV and 0.4–10 eV, respectively. Other transition systems are relatively weaker, thus contributing less to the total cross sections.

3.3. Rate Coefficients

The rate coefficients are computed by integrating the cross sections over the Maxwell–Boltzmann distribution (Equation (8)) for temperatures in the range of 10–10,000 K. The results for the 33 transition systems mentioned above and the total rate coefficients of singlet and triplet states are shown in Figure 7. Plainly, the total rate coefficient of the quintet states contributes little to the total rate coefficient, as depicted in Figure 8. Thus, the rate coefficients for the transitions between quintet states are not displayed individually. The $a^3\Sigma^+ \rightarrow a^3\Pi$ and $d^3\Delta \rightarrow a^3\Pi$ transitions make significant contributions to the radiative association for $T=10$ –30 K. The total rate coefficient at low temperatures is estimated to be about $10^{-18} \text{ cm}^3 \text{ s}^{-1}$. In addition, the $A^1\Pi \rightarrow X^1\Sigma^+$ transition gradually dominates with the increment of temperature up to 10,000 K. The $B^1\Sigma^+ \rightarrow X^1\Sigma^+$ transition goes up sharply for temperatures larger than 100 K,

and reaches a value very close to that of the $A^1\Pi \rightarrow X^1\Sigma^+$ transition around 1000 K.

The results are compared with those obtained by Gustafsson & Nyman (2015) and there is a discrepancy between our and Gustafsson & Nyman's total rate coefficient, as shown in Figure 8. Our total rate coefficient at low temperatures is larger than that of Gustafsson & Nyman (2015) because we considered all dipole-allowed transitions between singlet, triplet, and quintet states converging to the C ($2s^22p^2\ ^3P$) and O ($2s^22p^4\ ^3P$) dissociation limit, while Gustafsson & Nyman only considered three transition processes including $X^1\Sigma^+ \rightarrow X^1\Sigma^+$, $A^1\Pi \rightarrow X^1\Sigma^+$, and $B^1\Sigma^+ \rightarrow X^1\Sigma^+$. The deviation decreases as the temperature increases, which is three orders of magnitude at 10 K and one order of magnitude at 30 K, and almost disappears for temperatures larger than 6000 K, which mainly results from the contribution of the $A^1\Pi \rightarrow X^1\Sigma^+$ and $B^1\Sigma^+ \rightarrow X^1\Sigma^+$ transitions both considered by our calculations and those of Gustafsson & Nyman. Meanwhile, the slight discrepancies in the $A^1\Pi \rightarrow X^1\Sigma^+$ and $B^1\Sigma^+ \rightarrow X^1\Sigma^+$ transitions could be due to the PECs and TDMs. The PECs and TDMs used by Gustafsson & Nyman are different from ours. The radiative lifetime of the $A^1\Pi$ state was calculated to further verify the accuracy of our PECs and TDMs, as depicted in Table 3.

The total rate coefficient for CO radiative association can be approximated using the following three-parameter Kooij function (Gustafsson & Nyman 2015):

$$k(T) = A \left(\frac{T}{300} \right)^\alpha e^{-\beta/T}, \quad (10)$$

where A , α , and β are fitting parameters. The rate coefficient curve is divided into eight temperature intervals, and the fitting parameters are summarized in Table 4. The fitted rate coefficient deviates from our calculated one by less than 1%.

The rate coefficients can improve the chemical models of CO formation in the low-density region of the interstellar medium. Lepp et al. (1990) summarized previous research and deduced that the formation of CO may be accomplished directly by the radiative association. Subsequently, Dalgarno et al. (1990) explored an alternative calculation of the rate coefficients and concluded the major source of CO is the direct radiative association of C and O. When modeling the density and abundance profiles of CO, Gearhart et al. (1999) adopted the reaction rate coefficients of CO radiative association given by

Dalgarno et al. (1990). The CO formation is most sensitive to the rate coefficients of radiative association. Therefore, our new rate coefficients may improve the accuracy of determining the CO column density and abundance profiles. In addition, rate coefficients for the radiative association of C and O at different temperatures are required to model the CO formation in various astrophysical environments, such as the interstellar clouds and the turbulent interstellar medium (Prasad & Huntress 1980; Glover et al. 2010).

4. Conclusions

In this work, we have calculated the cross sections and rate coefficients for the formation of CO through the radiative association in the collision of C ($2s^22p^2\ ^3P$) and O ($2s^22p^4\ ^3P$). All dipole-allowed transitions between singlet, triplet, and quintet states converging to the first dissociation limit have been considered based on a new set of PECs, PDMs, and TDMs calculated at the icMRCI+Q/aug-cc-pwCV5Z-DK level of theory. Our results suggest that the $a^3\Sigma^+ \rightarrow a^3\Pi$ and $d^3\Delta \rightarrow a^3\Pi$ transitions make significant contributions to the radiative association for $T = 10\text{--}30$ K. The total rate coefficient at low temperatures is estimated to be about $10^{-18}\text{ cm}^3\text{ s}^{-1}$, which is larger than that of Gustafsson & Nyman (2015). The total rate coefficient for the radiative association of CO is of the order of $1.18 \times 10^{-18}\text{--}1.31 \times 10^{-16}\text{ cm}^3\text{ s}^{-1}$ for temperatures of $10\text{--}10,000$ K. The calculated cross sections and rate coefficients may improve the understanding of the CO chemical evolution in some celestial bodies.

This work is sponsored by the National Natural Science Foundation of China (52106098), Natural Science Foundation of Shandong Province (ZR2021QE021), China Postdoctoral Science Foundation (2021M701977), Postdoctoral Innovation Project of Shandong Province and Postdoctoral Applied Research Project of Qingdao City. The scientific calculations in this paper were done on the HPC Cloud Platform of Shandong University.

Appendix

The fitted spectroscopic constants are summarized in Table 5, together with previous experimental and theoretical ones. The rate coefficients are given in Tables 6–10 and can also be obtained online at <https://dr-zhi-qin.github.io/personal/Database.html>.

Table 5
Spectroscopic Constants of CO Compared with Available Experimental and Theoretical Results

State	$D_e(\text{eV})$	$T_e(\text{cm}^{-1})$	$R_e(\text{\AA})$	$\omega_e(\text{cm}^{-1})$	$\omega_e\chi_e(\text{cm}^{-1})$	$B_e(\text{cm}^{-1})$	$10^2\alpha_e(\text{cm}^{-1})$
X ¹ Σ^+	11.2248	0	1.1309	2169.75	13.43	1.9236	1.745
Expt. ^a	11.2241	0	1.1283	2169.81	13.29	1.9313	1.750
Expt. ^b	11.2241	0	1.1282	2169.76	13.29	1.9316	1.751
Expt. ^c	...	0	1.1282	2169.80	13.30
Calc. ^d	...	0	1.1180	2351.70	10.80	1.9650	...
Calc. ^e	...	0	1.1393	2151.60	12.90
Calc. ^f	...	0	1.1310	2178.00	13.00
Calc. ^g	...	0	1.1333	2134.00	13.70	1.9140	1.820
Calc. ^h	11.2283	0	1.1306	2169.19	14.10	1.9278	1.602
a ³ Π	5.1930	48695.1	1.2081	1740.67	13.83	1.6872	1.838
Expt. ^a	5.1877	48686.7	1.2057	1743.41	14.36	1.6912	1.904
Expt. ⁱ	1738.26	14.25
Calc. ^d	...	48702.0	1.1880	1967.90	12.80	1.7430	...
Calc. ^g	...	48652.1	1.2016	1766.00	15.10	1.7030	1.960
Calc. ^h	5.1617	48861.2	1.2062	1743.35	13.59	1.6897	2.096
Calc. ^j	...	48419.8	1.2090	1757.10	25.40
a ³ Σ^+	4.3068	55520.4	1.3600	1236.79	10.01	1.3466	1.917
Expt. ^a	4.3026	55825.5	1.3523	1228.60	10.47	1.3446	1.892
Expt. ^o	...	55823.0	1.3520	1230.70	11.00	1.3450	...
Calc. ^d	...	57744.0	1.3020	1654.10	-0.60	1.4510	...
Calc. ^g	...	54372.2	1.3857	1110.00	16.90	1.2800	2.070
Calc. ^h	4.3029	55861.1	1.3575	1212.97	9.19	1.3299	1.667
Calc. ^k	...	55540.0	1.3450	1240.00
d ³ Δ	3.6084	60818.7	1.3700	1188.60	10.05	1.3084	1.774
Expt. ^a	3.6462	61120.1	1.3696	1171.94	10.64	1.3108	1.782
Calc. ^d	...	63692.0	1.3080	1626.70	-1.00	1.4370	...
Calc. ^g	...	60619.6	1.3773	1166.00	12.70	1.2960	1.740
Calc. ^h	3.6421	61158.6	1.3709	1168.16	10.27	1.3034	1.743
Calc. ^k	...	60560.0	1.3730	1150.00
e ³ Σ^-	3.2804	63985.1	1.3802	1123.03	10.69	1.2807	1.782
Expt. ^a	3.2606	64230.2	1.3840	1117.94	10.69	1.2836	1.753
Expt. ^o	...	65340.0	1.3930	1094.00	9.60	1.2660	...
Calc. ^d	...	69617.0	1.3140	1569.90	-1.20	1.4230	...
Calc. ^g	...	65665.0	1.3782	1162.00	11.80	1.2940	1.700
Calc. ^h	3.2566	64259.8	1.3856	1108.43	9.48	1.2745	1.723
Calc. ^k	...	62710.0	1.3900	1100.00
A ¹ Π	3.1755	64864.9	1.2370	1529.22	17.97	1.6109	2.426
Expt. ^a	3.1557	65075.8	1.2353	1518.24	19.40	1.6115	2.325
Expt. ^l	1.6042	...
Calc. ^e	...	66782.7	1.2499	1475.00	18.90
Calc. ^g	...	65587.8	1.2342	1506.00	19.30	1.6140	1.740
Calc. ^h	3.1376	65175.0	1.2382	1514.72	16.78	1.6091	2.413
Calc. ^m	...	64755.7	1.2370	1461.20	4.40
I ¹ Σ^-	3.1462	65064.6	1.3961	1070.45	10.81	1.2675	1.801
Expt. ^a	3.1547	65084.4	1.3911	1092.22	10.70	1.2705	1.848
Calc. ^g	...	65912.6	1.3782	1162.00	11.80	1.2940	1.700
Calc. ^h	3.1567	65079.7	1.3937	1079.20	9.50	1.2630	1.750
Calc. ^j	...	65089.4	1.3950	1114.70	12.10
D ¹ Δ	3.0359	65963.2	1.4021	1052.53	10.94	1.2570	1.827
Expt. ^a	3.0420	65928.0	1.3990	1094.00	10.20	1.2570	1.700
Calc. ^g	...	69503.2	1.3786	1157.00	11.70	1.2940	1.740
Calc. ^h	3.0458	65965.5	1.3999	1052.19	9.47	1.2517	1.753
Calc. ⁿ	...	65977.0	1.4080	1038.00	11.90
b ³ Σ^+	2.9366	84074.9	1.1103	2218.68	105.31	1.9810	4.466
Expt. ^a	...	83814.0	1.1130	2199.30	...	1.9860	4.200
Expt. ^p	...	83776.8	1.1500	2335.00
Calc. ^q	...	83462.2	1.1140	1879.00
I ⁵ Π	0.7822	84248.6	1.4545	919.80	1.57	1.1304	1.006
B ¹ Σ^+	0.8519	86736.0	1.1200	2135.32	13.52	1.9564	2.575
Expt. ^a	...	86945.2	1.1197	2122.70	15.22	1.9612	2.610
Expt. ^r	...	86926.9	1.1197	2161.70	39.80
Calc. ^e	...	84930.1	1.1298	2166.40	30.50
Calc. ^m	...	87292.8	1.1240	2093.00	15.70
Calc. ^h	0.7984	87072.2	1.1238	2131.77	10.00	1.8468	0.665

Table 5
(Continued)

State	$D_e(\text{eV})$	$T_e(\text{cm}^{-1})$	$R_e(\text{\AA})$	$\omega_e(\text{cm}^{-1})$	$\omega_e\chi_e(\text{cm}^{-1})$	$B_e(\text{cm}^{-1})$	$10^2\alpha_e(\text{cm}^{-1})$
$c^3\Pi$	1.1045	92952.7	1.1177	2180.79	47.72	1.9722	3.235
Expt. ^a	...	93158.5	1.1270	1.9533	1.960
Expt. ^s	...	92076.9	1.1203	2190.00
Calc. ^m	...	91948.5	1.1160	1948.90
$E^1\Pi$	1.4972	93062.9	1.1206	2169.11	11.71	1.9567	1.349
Expt. ^a	...	92903.0	1.1152	2153.80	42.00	1.9771	2.540
Expt. ^t	...	92929.9	1.1221	2152.90
Calc. ^e	...	90979.3	1.1319	2175.00	19.60
Calc. ^m	...	92649.4	1.1220	2127.60
$1^3\Sigma^-$	0.5713	117486.2	1.3672	1329.16	52.11	1.3391	2.370

Notes.^a Huber & Herzberg (1979).^b Le Floch (1991).^c George et al. (1994).^d Nesbet (1965).^e Cooper & Kirby (1987).^f Chantranupong et al. (1992).^g Falzon et al. (2006).^h Zhang & Shi (2021).ⁱ Prasad et al. (1987).^j Cooper & Langhoff (1981).^k Hall et al. (1973).^l Le Floch et al. (1987).^m Vázquez et al. (2009).ⁿ Rosenkrantz & Kirby (1989).^o Herzberg & Hugo (1955).^p Wan & Langhoff (1991).^q Marshall (2008).^r Eidelsberg & Rostas (1990).^s Baker (2005).^t Cacciani & Ubachs (2004).**Table 6**
Rate Coefficients ($\text{cm}^3 \text{s}^{-1}$) for CO

$T(\text{K})$	A–A	A–D	A–I	A–X	B–A	B–X	D–A	D–D	E–A
1	1.61352E-29	1.42970E-26	1.71298E-27	4.24883E-24	1.74857E-31	2.17220E-21	1.20364E-19	1.09522E-20	3.34834E-32
2	2.07001E-29	1.83908E-26	2.22579E-27	6.13197E-24	6.70729E-32	1.00100E-21	4.59356E-20	4.16569E-21	2.11049E-32
3	2.39400E-29	2.02240E-26	2.51780E-27	7.18633E-24	3.87761E-32	6.92323E-22	2.67941E-20	2.42517E-21	2.36490E-32
4	2.60938E-29	2.11657E-26	2.69669E-27	7.86102E-24	2.65864E-32	5.56942E-22	1.87228E-20	1.69359E-21	3.10705E-32
⋮
9999	7.56636E-23	3.26308E-21	4.60221E-21	5.84345E-17	1.08589E-19	5.42341E-17	4.53358E-21	3.46811E-22	5.99409E-20
10000	7.56619E-23	3.26285E-21	4.60190E-21	5.84356E-17	1.08589E-19	5.42352E-17	4.53340E-21	3.46793E-22	5.99517E-20

(This table is available in its entirety in machine-readable form.)

Table 7
Rate Coefficients ($\text{cm}^3 \text{s}^{-1}$) for CO

$T(\text{K})$	E–B	E–D	E–I	E–X	I–A	I–I	X–A	X–X	Total (Singlets)
1	1.58979E-30	1.72255E-31	7.57065E-31	5.80656E-31	1.78248E-20	6.35517E-22	5.00385E-24	5.32647E-22	1.5249E-19
2	8.83830E-31	1.09867E-31	4.76964E-31	3.26885E-31	9.25368E-21	3.3128E-22	1.91050E-24	4.55523E-22	6.11509E-20
3	7.66263E-31	1.29383E-31	5.47232E-31	2.93137E-31	2.56941E-22	2.56941E-22	1.09653E-24	4.91036E-22	3.78164E-20
4	7.77662E-31	1.81529E-31	7.45364E-31	3.10591E-31	2.27772E-22	2.27772E-22	7.55717E-25	5.55351E-22	2.80786E-20
⋮
9999	3.00488E-23	5.67967E-20	8.83655E-20	7.81155E-18	5.76149E-21	1.38460E-22	1.20864E-25	7.75279E-22	1.20813E-16
10000	3.00507E-23	5.68076E-20	8.83831E-20	7.81346E-18	5.76128E-21	1.38451E-22	1.20868E-25	7.75244E-22	1.20817E-16

(This table is available in its entirety in machine-readable form.)

Table 8
Rate Coefficients ($\text{cm}^3 \text{s}^{-1}$) for CO

$T(\text{K})$	a'-a	a'-a'	a-a	a-a'	a-d	a-e	b-a	b-a'
1	4.08228E-17	8.42456E-21	6.50802E-25	3.41537E-24	8.79878E-25	5.99166E-25	8.50212E-32	5.24923E-21
2	1.48475E-17	3.36224E-21	2.66677E-25	2.52507E-24	6.48234E-25	4.49620E-25	9.23602E-32	2.02438E-21
3	8.34358E-18	2.09547E-21	1.67938E-25	2.17233E-24	5.56465E-25	3.89690E-25	1.00875E-31	1.16427E-21
4	5.62753E-18	1.57845E-21	1.27172E-25	2.00283E-24	5.12484E-25	3.60222E-25	1.07158E-31	7.96156E-22
:
9999	5.60077E-19	5.09611E-22	1.07063E-22	8.35006E-21	1.34166E-21	5.93039E-22	2.56779E-19	1.63362E-18
10000	5.60063E-19	5.09581E-22	1.07057E-22	8.34950E-21	1.34154E-21	5.92981E-22	2.56861E-19	1.63373E-18

(This table is available in its entirety in machine-readable form.)

Table 9
Rate Coefficients ($\text{cm}^3 \text{s}^{-1}$) for CO

$T(\text{K})$	c-a	c-a'	c-d	c-e	d-a	d-d	e-a	e-e	Total (Triplets)
1	4.14637E-33	2.74263E-31	4.90110E-31	1.30340E-31	1.90158E-18	2.05760E-20	4.94152E-19	1.50618E-21	4.32543E-17
2	5.24768E-33	2.74484E-31	5.90617E-31	1.57374E-31	8.23988E-19	8.21945E-21	2.31104E-19	8.88896E-22	1.59171E-17
3	1.03449E-32	3.82724E-31	1.00719E-30	2.68438E-31	5.06873E-21	2.56941E-22	1.64173E-19	7.33177E-22	9.07821E-18
4	1.93219E-32	5.19219E-31	1.63830E-30	4.36893E-31	3.74449E-21	2.27772E-22	1.36591E-19	6.72217E-22	6.22997E-18
:
9999	6.14850E-18	6.41134E-19	1.69341E-19	2.05173E-19	4.77326E-19	9.87089E-22	1.47936E-19	3.81308E-22	1.02522E-17
10000	6.14889E-18	6.41175E-19	1.69350E-19	2.05183E-19	4.77317E-19	9.87027E-22	1.47934E-19	3.81285E-22	1.02528E-17



(This table is available in its entirety in machine-readable form.)

Table 10
Rate Coefficients ($\text{cm}^3 \text{s}^{-1}$) for CO

$T(\text{K})$	$1^5\Delta - 1^5\Pi$	$1^5\Pi - 1^5\Pi$	$1^5\Sigma^- - 1^5\Pi$	$1^5\Sigma^+ - 1^5\Pi$	$2^5\Pi - 1^5\Pi$	$2^5\Sigma^+ - 1^5\Pi$	Total (Quintets)	Total
1	2.14189E-21	1.3054E-25	2.04468E-27	5.22507E-24	7.86865E-32	2.75419E-30	2.14724E-21	4.34089E-17
2	1.13431E-21	4.83506E-26	7.48576E-28	2.05567E-24	4.19906E-32	1.74905E-30	1.13642E-21	1.59794E-17
3	8.7071E-22	2.73383E-26	4.20199E-28	1.19906E-24	5.82682E-32	1.42822E-30	8.71936E-22	9.1169E-18
4	7.62854E-22	1.84323E-26	2.81725E-28	8.26718E-25	1.14911E-31	1.2818E-30	7.63699E-22	6.25881E-18
:
9999	3.81309E-22	9.53482E-25	2.7553E-22	1.60269E-20	6.9178E-20	9.74427E-22	8.68372E-20	1.31152E-16
10000	3.81286E-22	9.53376E-25	2.75611E-22	1.60283E-20	6.9209E-20	9.7486E-22	8.68701E-20	1.31157E-16

(This table is available in its entirety in machine-readable form.)

ORCID iDs

Zhi Qin  <https://orcid.org/0000-0001-7995-0006>
 Linhua Liu  <https://orcid.org/0000-0002-4547-7676>

References

- Andreazza, C., de Almeida, A., & Borin, A. 2016, *MNRAS*, 457, 3096
 Antipov, S. V., Gustafsson, M., & Nyman, G. 2013, *MNRAS*, 430, 946
 Babb, J., & Dalgarno, A. 1995, *PhRvA*, 51, 3021
 Bai, T., Qin, Z., & Liu, L. 2021, *MNRAS*, 500, 2496
 Bai, T., Qin, Z., & Liu, L. 2022, *MNRAS*, 510, 1649
 Baker, J. 2005, *JMoSp*, 234, 75
 Cacciani, P., & Ubachs, W. 2004, *JMoSp*, 225, 62
 Cairnie, M., Forrey, R., Babb, J., Stancil, P., & McLaughlin, B. 2017, *MNRAS*, 471, 2481
 Carlson, T. A., uric, N., Erman, P., & Larsson, M. 1978, *ZPhyA*, 287, 123
 Chantranupong, L., Bhanuprakash, K., Honigmann, M., Hirsch, G., & Buenker, R. J. 1992, *CP*, 161, 351
 Cheng, J., Zhang, H., & Cheng, X. 2018, *ApJ*, 859, 19
 Chervenak, J., & Anderson, R. 1971, *JOSA*, 61, 952
 Cooper, D. L., & Kirby, K. 1987, *JChPh*, 87, 424
 Cooper, D. M., & Langhoff, S. R. 1981, *JChPh*, 74, 1200
 Dalgarno, A., Du, M., & You, J. 1990, *ApJ*, 349, 675
 De Jong, W. A., Harrison, R. J., & Dixon, D. A. 2001, *JChPh*, 114, 48
 Dunning, T. H., Jr. 1989, *JChPh*, 90, 1007
 Eidelsberg, M., & Rostas, F. 1990, *A&A*, 235, 472
 Eidelsberg, M., Rostas, F., Breton, J., & Thieblemont, B. 1992, *JChPh*, 96, 5585
 Falzon, C. T., Chong, D. P., & Wang, F. 2006, *JCoCh*, 27, 163
 Field, R., & Benoist, d. 1983, *JChPh*, 78, 2838
 Forrey, R., Babb, J., Stancil, P., & McLaughlin, B. 2018, *MNRAS*, 479, 4727
 Forrey, R. C. 2015, *JChPh*, 143, 024101
 Franz, J., Gustafsson, M., & Nyman, G. 2011, *MNRAS*, 414, 3547
 Gearhart, R. A., Wheeler, J. C., & Swartz, D. A. 1999, *ApJ*, 510, 944
 George, T., Urban, W., & Lefloch, A. 1994, *JMoSp*, 165, 500
 Glassgold, A. 1996, *ARA&A*, 34, 241
 Glassgold, A., Mamon, G., & Huggins, P. 1991, *ApJ*, 373, 254
 Glover, S. C., Federrath, C., Mac Low, M.-M., & Klessen, R. S. 2010, *MNRAS*, 404, 2
 Gustafsson, M. 2020, *JChPh*, 153, 114305
 Gustafsson, M., & Forrey, R. C. 2019, *JChPh*, 150, 224301
 Gustafsson, M., & Nyman, G. 2015, *MNRAS*, 448, 2562
 Hall, J., Schamps, J., Robbe, J., & Lefebvre-Brion, H. 1973, *JChPh*, 59, 3271
 Hansson, A., & Watson, J. K. 2005, *JMoSp*, 233, 169

- Herbst, E., & Bates, D. R. 1988, *ApJ*, **329**, 410
- Herzberg, G., & Hugo, T. 1955, *CaJPh*, **33**, 757
- Hesser, J. E. 1968, *JChPh*, **48**, 2518
- Huber, K., & Herzberg, G. 1979, *Molecular Spectra and Molecular Structure: IV. Constants of Diatomic Molecules* (Berlin: Springer-Verlag)
- Imhof, R., & Read, F. 1971, *CPL*, **11**, 326
- Johnson, B. R. 1977, *JChPh*, **67**, 4086
- Johnson, B. R. 1978, *JChPh*, **69**, 4678
- Julienne, P., & Krauss, M. 1973, in *Molecules in the Galactic Environment*, ed. M. A. Gordon & L. E. Snyder (New York: Wiley and Sons, Inc), 353
- Kirby, K., & Cooper, D. L. 1989, *JChPh*, **90**, 4895
- Knowles, P. J., & Werner, H.-J. 1985, *CPL*, **115**, 259
- Knowles, P. J., & Werner, H.-J. 1988, *CPL*, **145**, 514
- Knowles, P. J., & Werner, H.-J. 1992, *AcTC*, **84**, 95
- Langer, W. D., & Glassgold, A. 1990, *ApJ*, **352**, 123
- Le Floch, A. 1991, *MolPh*, **72**, 133
- Le Floch, A., Launay, F., Rostas, J., et al. 1987, *JMoSp*, **121**, 337
- Lepp, S., Dalgarno, A., & McCray, R. 1990, *ApJ*, **358**, 262
- Liu, W., & Dalgarno, A. 1994, *ApJ*, **428**, 769
- Marshall, D. 2008, *JQSRT*, **109**, 2546
- Nesbet, R. 1965, *JChPh*, **43**, 4403
- Nyman, G., Gustafsson, M., & Antipov, S. V. 2015, *IRPC*, **34**, 385
- Peterson, K. A., & Dunning, T. H., Jr. 2002, *JChPh*, **117**, 10548
- Prasad, C., Bhale, G., & Reddy, S. P. 1987, *JMoSp*, **121**, 261
- Prasad, S., & Huntress, W., Jr. 1980, *ApJS*, **43**, 1
- Qin, Z., Bai, T., & Liu, L. 2021, *MNRAS*, **507**, 2930
- Rawlings, J. 1988, *MNRAS*, **232**, 507
- Reiher, M., & Wolf, A. 2004, *JChPh*, **121**, 2037
- Reiher, v., & Wolf, A. 2004, *JChPh*, **121**, 10945
- Rosenkrantz, M., & Kirby, K. 1989, *JChPh*, **90**, 6528
- Shamasundar, K., Knizia, G., & Werner, H.-J. 2011, *JChPh*, **135**, 054101
- Szabó, P., & Gustafsson, M. 2017, *JChPh*, **147**, 094308
- Vázquez, G., Amero, J., Liebermann, H., & Lefebvre-Brion, H. 2009, *JPCA*, **113**, 13395
- Wan, B., & Langhoff, H. 1991, *ZPhyD*, **21**, 245
- Watson, J. K. 2008, *JMoSp*, **252**, 5
- Werner, H., Knowles, P., Knizia, G., et al. 2015, MOLPRO, a package of ab initio programs, <http://www.molpro.net>
- Werner, H.-J., & Knowles, P. J. 1985, *JChPh*, **82**, 5053
- Werner, H.-J., Knowles, P. J., Manby, F. R., et al. 2020, *JChPh*, **152**, 144107
- Werner, v. J., & Knowles, P. J. 1988, *JChPh*, **89**, 5803
- Zámečníková, M., Gustafsson, M., Nyman, G., & Soldán, P. 2020, *MNRAS*, **492**, 3794
- Zhang, M., & Shi, D. 2021, *Comput. Theor. Chem*, **1202**, 113302